

¹ Highlights

² **Asymmetric light absorption in a nature-like chiral microcavity**

³ Larisa E. Tyryshkina, Alexandr V. Shabanov, Rashid G. Bikbaev, Natalya
⁴ V. Rudakova, Dmitry P. Fedchenko, Stepan Ya. Vetrov, Ivan V. Timofeev

- ⁵ • In cholesteric liquid crystal we demonstrate the dependence of the res-
⁶ onant absorptance of light with co-handed circular polarization on the
⁷ defect layer position.
- ⁸ • Resonant absorption spectra for various cholesteric thicknesses are cal-
⁹ culated by three different methods.
- ¹⁰ • Temporal coupled-mode theory is used to explain symmetry break-
¹¹ ing in absorption, depending on the position of the defect within the
¹² cholesteric liquid crystal structure.

¹³ Asymmetric light absorption in a nature-like chiral
¹⁴ microcavity

¹⁵ Larisa E. Tyryshkina^{a,b}, Alexandr V. Shabanov^a, Rashid G. Bikbaev^{a,b},
¹⁶ Natalya V. Rudakova^{a,b}, Dmitry P. Fedchenko^{a,b}, Stepan Ya. Vetrov^{b,a},
¹⁷ Ivan V. Timofeev^{a,b,c}

^a*Kirensky Institute of Physics Federal Research Center KSC SB RAS Krasnoyarsk
660036 Russia*

^b*Siberian Federal University Krasnoyarsk 660041 Russia*

^c*tiv@iph.krasn.ru*

¹⁸ **Abstract**

In 1896, Lorenz published a well-known reciprocity theorem to demonstrate that the transmission of a non-magnetic linear stationary photonic structure is equal in both forward and reverse directions. However, the absorption of an asymmetric structure does not meet this condition. This symmetry breaking explains the spatial asymmetry in natural light-harvesting complexes and paves the way to novel spatially asymmetric photonic structures with optimal optical energy conversion. Here we consider a cholesteric liquid crystal layer as an example of a self-organizing one-dimensional photonic crystal with helical permittivity tensor. The optimal distribution of absorbing material inside the cholesteric is shown to be spatially asymmetric. The absorptance formula is found in the framework of the temporal coupled-mode theory and approved both by the Berreman method and anisotropic transfer matrix numerical calculations.

¹⁹ *Keywords:* reciprocity theorem, temporal coupled modes theory,
²⁰ anisotropic transfer matrix, photonic crystal, cholesteric liquid crystal,
²¹ light-harvesting

²² **1. Introduction**

²³ The material with a photonic bandgap in its energy spectrum is called
²⁴ a photonic crystal (PhC) [1, 2]. The dielectric constant of this material is
²⁵ modulated in space, with a periodicity that allows for Bragg diffraction of

26 light. The theory of light propagation in PhC is closely related to the quan-
27 tum theory of electron behavior in crystals which allows the use of concepts
28 like Bloch waves and Brillouin zones to describe the behavior of light in these
29 materials. Interest in PhC is caused by the possibility of creating lasers[3, 4],
30 switches [5], and sensors [6]. New opportunities for manipulating the opti-
31 cal properties of PhC arise from incorporating liquid crystals [7], nonlinear
32 media [8], or resonant materials [9, 10].

33 PhCs can also be found in nature [11, 12]. One example of a natural
34 PhC is the well-known mineral opal [13, 14, 15]. Its structure is a cubic
35 lattice formed by silica spheres close in diameter, arranged in a face-centered
36 pattern. This regular packing of spheres presents a superlattice of a three-
37 dimensional PhC. PhCs can be found in marine worms [16], whose needles
38 have an iridescent color that changes depending on the angle of light inci-
39 dence. The iridescence of the sea worms is similar to that of opals, due to the
40 diffraction of light on their complex microstructure. Structures with charac-
41 teristic dimensions of the order of the light wave are also responsible for the
42 iridescent coloring of the wings of some butterflies [17, 18]. It is worth noting
43 that these multilayered structures can also be found in plants [19]. The anal-
44 ysis of micrographs of plant iridoplasts [20] reveals the presence of structures
45 that could be considered as PhC with defects. The spatial position of the
46 defect layer within the structure may be asymmetric. Compared to the edge
47 mode, the defect mode enables a greater degree of localization of the light
48 field, which can lead to an increase in light absorption by plant cells during
49 the initial stages of photosynthesis. The results presented in [21] show that
50 the maximum value of light absorption and the electromagnetic field density
51 at the defect mode wavelength correspond to the asymmetric case with the
52 defective layer shifted towards the incident beam relative to the center. This
53 means that changing the position of the defect layer allows for controlling the
54 absorption at the defect mode wavelength. In natural iridoplasts the layered
55 structure is effectively sealed by the action of light [22], in similar artificially
56 manufactured PhC the asymmetry effect can be demonstrated by discretely
57 changing the number of periods to the left and right of the defect. However,
58 a smoother change in the position of the defective layer becomes possible
59 due to the use of a liquid crystal - a chiral medium - as a replacement for
60 the scalar photonic crystal. The optical properties of this medium can be
61 effectively controlled by applying an external electric field or by changing the
62 temperature.

63 This work aims to identify the effect of the asymmetric [23, 24] posi-

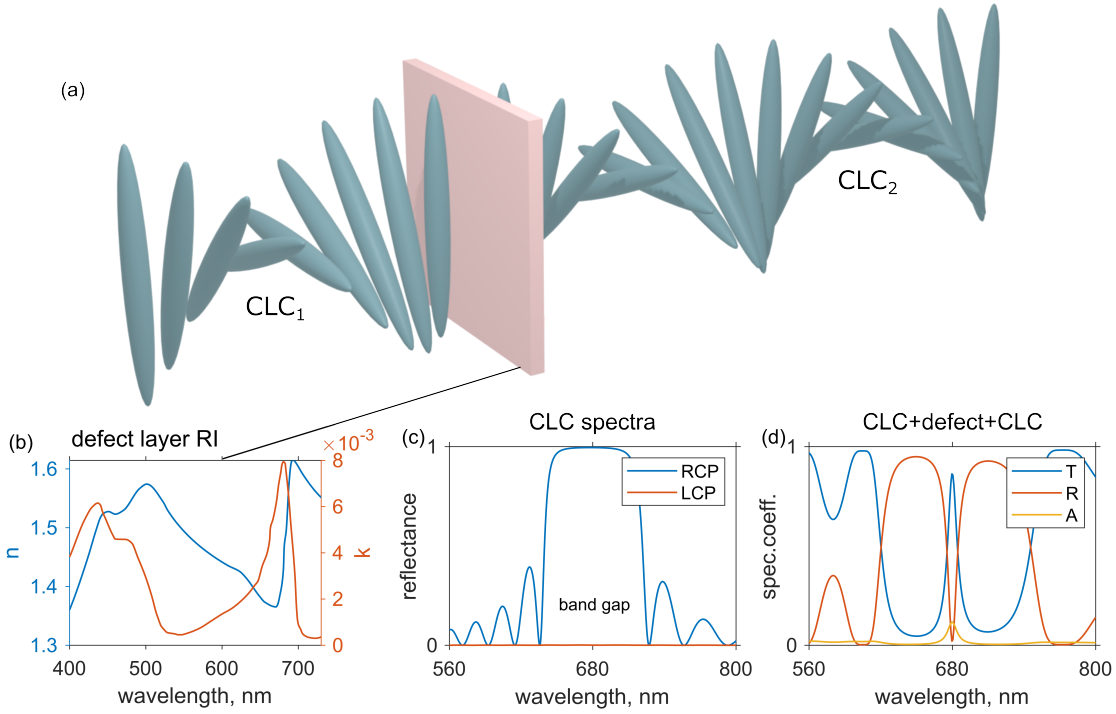


Figure 1: (a) Schematic representation of the structure under study; (b) Dependences of the real and imaginary parts of the complex refractive index of chlorophyll on light wavelength; (c) Reflection spectra of cholesteric liquid crystal (CLC) for right and left circular polarization; (d) Reflection, transmission and absorption spectra of a defective layer associated with two layers of the same thickness cholesterics, equal to $2 \mu\text{m}$.

tion of the defect on the optical properties and local characteristics of light
 waves propagating in a self-organizing photonic crystal. For this aim the
 cholesteric liquid crystal (chiral nematic) is considered because of its high
 optical birefringence [25, 26], nature-like viscous and anchoring properties
 [27]. Moreover, cholesterics possess high chirality, therefore they are capa-
 ble of focusing and deflecting light [28]. Due to the high density of states
 near the photonic band gap, the cholesteric demonstrates self-switching ef-
 fects [29] and luminescence enhancement [30] that makes it perspective for
 artificial photosynthesis applications.

2. Description of the model

The sketch view of the defect layer bounded by two cholesteric layers are
 presented in Figure 1. In this case, the defective layer mimics the thylakoid
 membrane of Selaginella erythropus bizonoplasts of [31, 22]. The real and
 imaginary parts of the complex refractive index of the defect layer depicted
 on Figure 1a were taken under the assumption of a low concentration of
 chlorophyll molecules [32], i.e. with its reduced imaginary part.

A cholesteric consists of elongated molecules oriented in space in the form
 of a twisting helix. Due to the helical symmetry of the cholesteric permittivity
 tensor and the periodicity of a helical pitch, the cholesteric liquid crystal is a
 one-dimensional photonic crystal with a photonic band gap in its spectrum.
 Such a chiral structure leads to diffraction of light circularly polarized in
 the helical twisting direction. The light with the oppositely twisted circular
 polarization does not diffract and is transmitted without significant changes.
 The cholesteric is characterized by the helix pitch p , thickness L and the
 ordinary and extraordinary refractive indices $n_e = \sqrt{\varepsilon_e} = 1.57$ and $n_o =$
 $\sqrt{\varepsilon_o} = 1.42$, respectively. The cholesteric permittivity tensors are:

$$\hat{\varepsilon}(z) = \varepsilon_m \begin{pmatrix} 1 + \delta \cos(qz) & \pm\delta \sin(2qz) & 0 \\ \pm\delta \sin(qz) & 1 - \delta \cos(qz) & 0 \\ 0 & 0 & 1 - \delta \end{pmatrix}, \quad (1)$$

where $q = 4\pi/p$, $\varepsilon_m = (\varepsilon_e + \varepsilon_o)/2$ and $\delta = (\varepsilon_e - \varepsilon_o)/(\varepsilon_e + \varepsilon_o)$.

3. Methods

3.1. Anisotropic transference matrix

Let's consider the anisotropic transfer matrix method for finding the spec-
 tra of an anisotropic photonic crystal (see, for example, [33]). The essence of

95 the transfer matrix method in an isotropic medium with normal light inci-
 96 dence is that the amplitudes of A and B waves traveling in the right and left
 97 directions, respectively, in the previous and current layers are self-consistent
 98 (see, for example, [34]):

$$A_{N-1} = \frac{1}{2} ((1+C)A_N e^{-ik_N z_N} + (1-C)B_N e^{ik_N z_N}), \quad (2)$$

$$B_{N-1} = \frac{1}{2} ((1-C)A_N e^{-ik_N z_N} + (1+C)B_N e^{ik_N z_N}), \quad (3)$$

99 where z is the local variable of the layer with the reference point placed on
 100 the right boundary, $k_N = \omega n_N / c$ is the wave number, and $C = n_N / n_{N-1}$.

101 In matrix language, the equations for the amplitudes A_{N-1}, B_{N-1} can be
 102 written as:

$$\begin{pmatrix} A_{N-1} \\ B_{N-1} \end{pmatrix} = \frac{1}{2} \begin{pmatrix} (1+C)e^{-ik_N z_N} & (1-C)e^{ik_N z_N} \\ (1-C)e^{-ik_N z_N} & (1+C)e^{ik_N z_N} \end{pmatrix} \begin{pmatrix} A_N \\ B_N \end{pmatrix} = M_2(C, k_N, z_N) \begin{pmatrix} A_N \\ B_N \end{pmatrix}, \quad (4)$$

103 with transfer matrix M_2 . For $C = 1$, the matrix M_2 belongs to the class
 104 $\text{SL}(2, C)$.

105 Transferring this approach to the case of anisotropic layers [33], we obtain
 106 an expression for the amplitude of the ordinary A_o, B_o and extraordinary
 107 A_e, B_e waves:

$$(A_{o_{N-1}} B_{o_{N-1}} A_{e_{N-1}} B_{e_{N-1}})^T = M_4 (A_{o_{N-1}} B_{o_{N-1}} A_{e_{N-1}} B_{e_{N-1}})^T, \quad (5)$$

108 where T denotes the operation of matrix transposition. The matrix M_4 from
 109 the last equality is a complex matrix of order 4, including four blocks of order
 110 2 filled with elements similar to those that make up the transfer matrix for
 111 an isotropic medium.

112 The anisotropic transfer matrix at a normal angle of incidence has the
 113 form:

$$M_4 = \begin{pmatrix} M_2 \left(\frac{k_{o_N}}{k_{o_{N-1}}}, k_{o_N}, z_N \right) & M_2 \left(\frac{k_{e_N}}{k_{o_{N-1}}}, k_{e_N}, z_N \right) \\ -M_2 \left(\frac{k_{e_{N-1}} n_{o_N}^2}{k_{o_N} n_{e_{N-1}}^2}, k_{o_N}, z_N \right) & M_2 \left(\frac{k_{e_{N-1}} n_{e_N}^2}{k_{e_N} n_{e_{N-1}}^2}, k_{e_N}, z_N \right) \end{pmatrix} S,$$

¹¹⁴ with a matrix S of the form

$$S = \begin{pmatrix} \cos(\delta) & \cos(\delta) & -\sin(\delta) & -\sin(\delta) \\ \cos(\delta) & \cos(\delta) & -\sin(\delta) & -\sin(\delta) \\ \sin(\delta) & \sin(\delta) & \cos(\delta) & \cos(\delta) \\ \sin(\delta) & \sin(\delta) & \cos(\delta) & \cos(\delta) \end{pmatrix}, \quad (6)$$

¹¹⁵ where δ is the azimuthal angle of rotation of the main optical axis along the
¹¹⁶ axis perpendicular to the boundary of the layers.

¹¹⁷ Let us consider a special case of an anisotropic layered medium with a
¹¹⁸ normal light incidence, rotating the main axis as it passes deep into the
¹¹⁹ structure and with the same layer thicknesses. In this case, we use the local
¹²⁰ Oseen basis [35], so the first axis in each layer coincides with the LC-director.
¹²¹ For example, these are cholesteric liquid crystals, C* smectics, Scholz filters.
¹²² Under these conditions, the refractive indices do not depend on the layer
¹²³ number, and therefore the matrix M_4 for a section of a cholesteric liquid
¹²⁴ crystal with a section length of L and a spiral pitch of L_0 is significantly
¹²⁵ simplified:

$$M_4 = \frac{1}{2} \begin{pmatrix} 2e^{-ik_o\Delta z} & 0 & p_o^e e^{-ik_e\Delta z} & m_o^e e^{ik_e\Delta z} \\ 0 & 2e^{ik_o\Delta z} & m_o^e e^{-ik_e\Delta z} & p_o^e e^{ik_e\Delta z} \\ p_o^e e^{-ik_o\Delta z} & m_o^e e^{-ik_o\Delta z} & 2e^{-ik_e\Delta z} & 0 \\ m_o^e e^{-ik_o\Delta z} & p_o^e e^{-ik_o\Delta z} & 0 & 2e^{ik_e\Delta z} \end{pmatrix} S, \quad (7)$$

¹²⁶ where $p_o^e = 1 + \frac{n_o}{n_e}$, $p_o^e = 1 + \frac{n_e}{n_o}$, $m_o^e = 1 - \frac{n_o}{n_e}$, $m_o^e = 1 - \frac{n_e}{n_o}$. When a photonic
¹²⁷ crystal is divided into N parts $\Delta z = L/N$, $\delta = 2\pi L/L_0 N$. When working
¹²⁸ with a large number of layers in a liquid crystal, it is advisable to represent
¹²⁹ the M_4 matrix in the form $M_4 = V\Lambda V^{-1}$, where Λ is the diagonal matrix of
¹³⁰ eigenvalues M , and V is a matrix whose columns are the eigenvectors of the
¹³¹ matrix M_4 . It is obvious that $M^N = V\Lambda^N V^{-1}$.

¹³² The characteristic equation for the matrix M_4 of cholesteric has the form

$$\lambda^4 + \alpha\lambda^3 + \beta\lambda^2 + \alpha\lambda + 1 = 0, \quad (8)$$

¹³³ the coefficients of the characteristic polynomial are expressed by the formulas:

$$\begin{aligned} \alpha &= -2 \cos(\delta)(\cos(k_o\Delta z) + \cos(k_e\Delta z)), \\ \beta &= (2 + 2 \cos^2(\delta)) \cos(k_o\Delta z) \cos(k_e\Delta z) - \\ &\quad - \sin^2(\delta) \sin(k_o\Delta z) \sin(k_e\Delta z) \left(\frac{n_o}{n_e} + \frac{n_e}{n_o} \right) + \cos^2(\delta), \end{aligned} \quad (9)$$

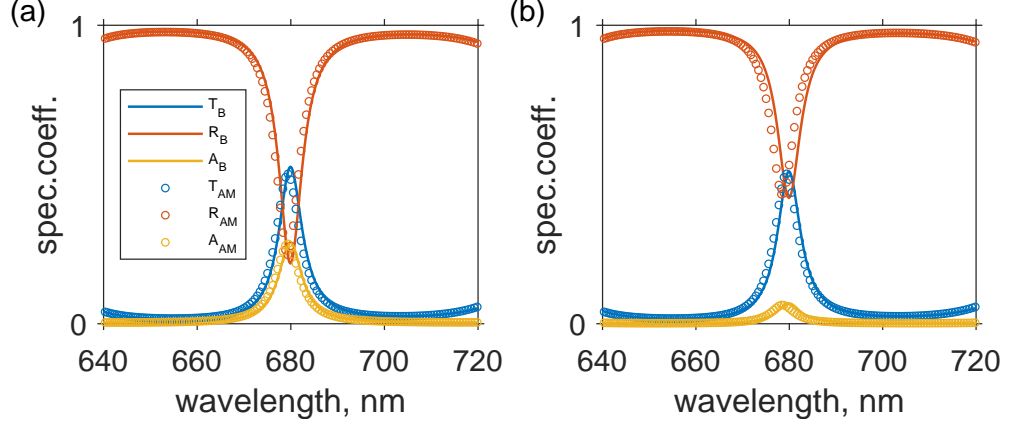


Figure 2: Reflection, transmission, and absorption spectra of the studied structure calculated by the Berreman method (solid lines) and the anisotropic matrix method (circles), with (a) $L_1 = 2 \mu\text{m}$ and $L_2 = 3 \mu\text{m}$, (b) $L_1 = 3 \mu\text{m}$ and $L_2 = 2 \mu\text{m}$.

and the roots:

$$\lambda_{1,2,3,4} = -\frac{\alpha}{4} \pm \frac{\sqrt{\alpha^2 - 4\beta^2 + 8}}{4} \pm \frac{\sqrt{2\alpha^2 - 2\alpha\sqrt{\alpha^2 - 4\beta^2 + 8} - 4\beta^2 - 8}}{4}.$$

The characteristic equation of the cholesteric is reciprocal (the sequence of coefficients $(1, \alpha, \beta, \alpha, 1)$ forms a palindrome). A similar property, for example, is possessed by the matrix of a unit (equal to one in norm) quaternion and the matrix commuting with the quaternion matrix, see [36], arising in the index theory of Toeplitz operators. The second matrix has the form:

$$A = \begin{pmatrix} a & -b & -c & -d \\ b & a & d & -c \\ c & -d & a & b \\ d & c & -b & a \end{pmatrix} \quad (10)$$

and its characteristic equation

$$\begin{aligned} \lambda^4 - 4a\lambda^3 + (4a^2 + 2(a^2 + b^2 + c^2 + d^2))\lambda^2 \\ - 4a(a^2 + b^2 + c^2 + d^2)\lambda + (a^2 + b^2 + c^2 + d^2)^2 = 0. \end{aligned}$$

¹⁴¹ If the determinant of the matrix $\det A = (a^2 + b^2 + c^2 + d^2)^2$ is equal to one,
¹⁴² then the characteristic equation becomes a palindrome.

¹⁴³ Reciprocal equations of degrees $2d$ and $2d + 1$ are reduced to solving
¹⁴⁴ the equation of degree d , which, according to the Abel–Ruffini theorem, is
¹⁴⁵ solvable in radicals for degrees $d \leq 4$. Consequently, any reciprocal equation
¹⁴⁶ of degree not exceeding 9 is solvable in radicals.

¹⁴⁷ Decompose the elements of the matrix M_4 into the Maclaurin series by
¹⁴⁸ Δz up to the first order:

$$\widetilde{M}_4 = \begin{pmatrix} 1 - k_o \Delta z & 0 & \pi p_o^e \frac{\Delta z}{L_0} & \pi m_o^e \frac{\Delta z}{L_0} \\ 0 & 1 + k_o \Delta z & \pi m_o^e \frac{\Delta z}{L_0} & \pi p_o^e \frac{\Delta z}{L_0} \\ -\pi p_e^o \frac{\Delta z}{L_0} & -\pi m_e^o \frac{\Delta z}{L_0} & 1 - k_e \Delta z & 0 \\ -\pi m_e^o \frac{\Delta z}{L_0} & -\pi p_e^o \frac{\Delta z}{L_0} & 0 & 1 + k_e \Delta z \end{pmatrix} \quad (11)$$

¹⁴⁹ where $p_e^o = 1 + \frac{n_o}{n_e}$, $p_o^e = 1 + \frac{n_e}{n_o}$, $m_e^o = 1 - \frac{n_o}{\tilde{n}_e}$, $m_o^e = 1 - \frac{n_e}{n_o}$. The roots λ_m of
¹⁵⁰ the characteristic equation of the matrix \widetilde{M}_4 have the form:

$$\lambda_m = 1 + \frac{\Delta z}{2L_o} F_m, \quad (12)$$

¹⁵¹ where

$$\begin{aligned} F_{1,2} &= \pm \sqrt{q_1 - q_2}, \quad F_{3,4} = \pm i \sqrt{q_1 + q_2}, \\ q_1 &= 2\omega L_o \sqrt{(\omega L_o)^2(n_e^2 - n_o^2)^2 + 32\pi^2(n_o^2 + n_e^2)}, \\ q_2 &= 2(\omega L_o)^2(n_o^2 + n_e^2) + 16\pi^2. \end{aligned}$$

¹⁵² and the eigenvectors X_m are expressed by the formulas:

$$\begin{aligned}
X_{1m} &= \frac{2i\pi\omega L_o \Delta z^2 (1 - n_e/n_o)}{D_1}, \\
X_{2m} &= \frac{2i\pi\omega L_o \Delta z^2 (1 + n_e/n_o)}{D_2}, \\
X_{3m} &= \frac{-\omega \Delta z n_e^2 (L_o^2 (\lambda_m - 1)^2 - \Delta z^2 ((\omega L_o \Delta z)^2 - 2\pi^2)))}{2\omega\pi^2 n_o^2 \Delta z^3 (n_e^2 - n_o^2)} \times \\
&\quad \times \frac{\lambda_m - 1}{2\omega\pi^2 n_o^2 \Delta z^3 (n_e^2 - n_o^2)} + \\
&\quad + \frac{-in_e (\Delta z^2 ((\omega L_o \Delta z)^2 + 4\pi^2) + L_o^2 (\lambda_m - 1)^2)}{2\omega\pi^2 n_o^2 \Delta z^3 (n_e^2 - n_o^2)} + \\
&\quad + \frac{1}{(n_e^2 - n_o^2)}, \\
X_{4m} &= 1,
\end{aligned}$$

¹⁵³ where

$$\begin{aligned}
D_1 &= L_o^2 ((\lambda_m - 1)^2 - (\omega \Delta z)^2 n_o n_e + \\
&\quad + i\omega \Delta z (n_o + n_e) (\lambda_m - 1)) + (2\pi \Delta z)^2,
\end{aligned}$$

¹⁵⁴ and

$$\begin{aligned}
D_2 &= L_o^2 ((\lambda_m - 1)^2 + (\omega \Delta z)^2 n_o n_e - \\
&\quad - i\omega \Delta z (n_o - n_e) (\lambda_m - 1)) + (2\pi \Delta z)^2.
\end{aligned}$$

¹⁵⁵ From the ratio $\lambda_m - 1 = (\Delta z / 2L_0) F_m$, we find that the value of Δz cancels in eigenvectors. Thus, the method is stable relative to the limit transition ¹⁵⁶ $\Delta z \rightarrow 0$. Let $n = L / \Delta z$, using the second remarkable limit, we obtain a ¹⁵⁷ formula for raising the diagonal matrix to a large degree (another approach ¹⁵⁸ based on the Ambartsumyan's method can be found in the works [37, 38, 39]: ¹⁵⁹

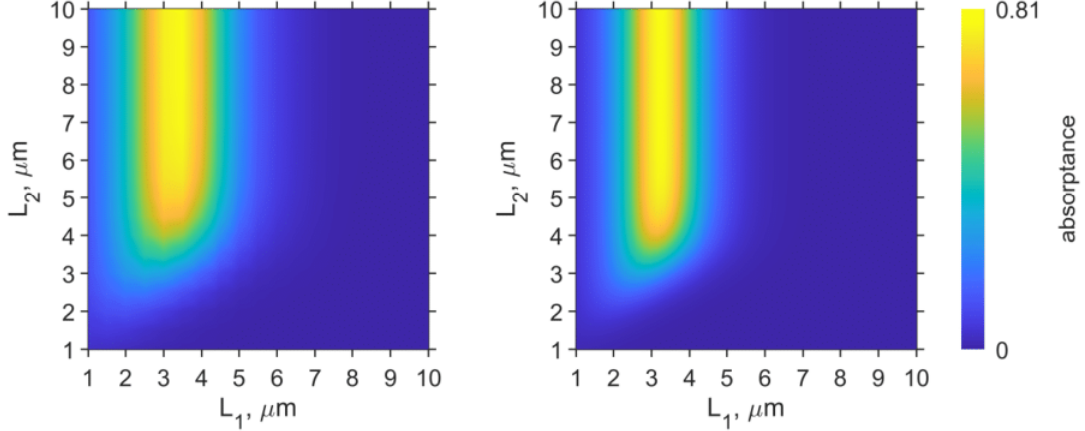


Figure 3: The dependences of the absorption coefficient at a wavelength of 680 nm on the thickness of cholesterics calculated using (a) the Berreman method and (b) the temporal couples mode theory, see (20). The colorbar is relevant for both subplots.

$$\lim_{n \rightarrow \infty} \begin{pmatrix} \lambda_1 & 0 & 0 & 0 \\ 0 & \lambda_2 & 0 & 0 \\ 0 & 0 & \lambda_3 & 0 \\ 0 & 0 & 0 & \lambda_4 \end{pmatrix}^n = \lim_{n \rightarrow \infty} \begin{pmatrix} \lambda_1^n & 0 & 0 & 0 \\ 0 & \lambda_2^n & 0 & 0 \\ 0 & 0 & \lambda_3^n & 0 \\ 0 & 0 & 0 & \lambda_4^n \end{pmatrix} = \\ = \begin{pmatrix} e^{\frac{LF_1}{2L_0}} & 0 & 0 & 0 \\ 0 & e^{\frac{LF_2}{2L_0}} & 0 & 0 \\ 0 & 0 & e^{\frac{LF_3}{2L_0}} & 0 \\ 0 & 0 & 0 & e^{\frac{LF_4}{2L_0}} \end{pmatrix}.$$

160 The limits for the eigenvalues of the matrix M_4 at $\Delta z \rightarrow 0$ exactly coincide
 161 with those given for the matrix of Maclaren approximations.

162 *3.2. Berreman transfer matrix method*

163 The spectral properties of the proposed structure and field distribution
 164 in it can be performed using the Berreman 4×4 transfer matrix method

[40]. The equation describing the propagation of light at frequency ω along the z axis normal to the structural layers has the form:

$$\frac{d\psi}{dz} = \frac{i\omega}{c} \Delta(z) \psi(z), \quad (13)$$

where $\psi(z) = (E_x, H_y, E_y, -H_x)^T$ and $\Delta(z)$ is the Berreman matrix, which depends on the dielectric function and the incident wave vector.

3.3. Temporal couples mode theory

Absorptance spectra of the investigated structure can be calculated by the temporal coupled-mode theory [41]. According to this theory, any resonance has an eigenmode frequency ω_0 and the number of ports N_l for the energy to be transferred into this state and to leak out of it. In the presented structure the energy loss in four channels is described by the relaxation times τ_{L_1} , τ_{L_2} , τ_ϕ and τ_{abs} (see. Figure 1). We assume the state to be described by the complex amplitude \mathcal{A} and energy $|\mathcal{A}|^2$. The state can be presented as the sum of all the incoming and outgoing energy fluxes with the amplitudes $s_{l\pm}$. If the energy outcome from the state is made through four channels then the total relaxation time is defined as $1/\tau = 1/\tau_{L_1} + 1/\tau_{L_2} + 1/\tau_\phi + 1/\tau_{abs}$. The change in the amplitude \mathcal{A} satisfies the equation:

$$d\mathcal{A}/dt = -i\omega_0\mathcal{A} - \mathcal{A}/\tau, \quad (14)$$

which has the following solution: $\mathcal{A}(t) = \mathcal{A}(0)e^{-i\omega_0 t - t/\tau}$.

Considering the incoming and outgoing energy fluxes $s_{l\pm}$, one can rewrite Equation (14) as:

$$d\mathcal{A}/dt = -i\omega_0\mathcal{A} - \sum_{l=1}^4 \mathcal{A}/\tau_l + \kappa_1 s_{1+} + \kappa_2 s_{2+}, \quad (15)$$

$$s_{l-} = s_{l+} + \kappa_l \mathcal{A}. \quad (16)$$

Here, κ_l is the value characterizing the coefficient of channel coupling, $\tau_{1,2,3,4} = \tau_{L_1,L_2,\phi,abs}$. It is sufficient to know the relaxation times τ_l and resonance frequency ω

$$\frac{d\mathcal{A}}{dt} = -i\omega_0\mathcal{A} - \sum_{l=1}^4 \mathcal{A}/\tau_l + \sum_{i=1}^2 \sqrt{\frac{2}{\tau_l}} s_{l+}, \quad (17)$$

¹⁸⁷ and the relationship of the flux amplitudes is determined by the expression:

$$s_{l-} = -s_{l+} + \sqrt{\frac{2}{\tau_l}} \mathcal{A}. \quad (18)$$

¹⁸⁸ The incident radiation with the frequency ω oscillates according to the
¹⁸⁹ harmonic form $e^{-i\omega t}$, making $d\mathcal{A}/dt = -i\omega\mathcal{A}$. Under these conditions, Equa-
¹⁹⁰ tions (17) and (18) with $s_{2+} = 0$ lead to:

$$\begin{aligned} -i\omega\mathcal{A} &= -i\omega_0\mathcal{A} - \sum_{l=1}^4 \mathcal{A}/\tau_l + \sum_{i=1}^2 \sqrt{\frac{2}{\tau_l}} s_{l+}, \\ s_{1-} &= -s_{1+} + \sqrt{\frac{2}{\tau_{L_1}}} \mathcal{A}, \\ s_{abs-} &= \sqrt{\frac{2}{\tau_{abs}}} \mathcal{A}, \end{aligned} \quad (19)$$

¹⁹¹ In the general case, the absorption coefficient at the resonance frequency
¹⁹² ($\omega = \omega_0$) is the ratio:

$$\begin{aligned} A_{L_1, L_2}(\omega_0) &= \frac{|s_{abs-}|^2}{|s_{1+}|^2} = \frac{(2/\tau_{abs})|\mathcal{A}|^2}{|s_{1+}|^2} = \\ &= \frac{4/(\tau_{L_1, L_2}\tau_{abs})}{(1/\tau_{L_1} + 1/\tau_{L_2} + 1/\tau_\phi + 1/\tau_{abs})^2}. \end{aligned} \quad (20)$$

¹⁹³ The absorptances in forward and reverse directions are inversely propor-
¹⁹⁴ tional to relaxation times as follows:

$$\frac{A_{L_1}}{A_{L_2}} = \frac{\tau_{L_2}}{\tau_{L_1}}. \quad (21)$$

¹⁹⁵ 4. Results

¹⁹⁶ Figure 1c shows the reflection spectrum of a single cholesteric liquid crys-
¹⁹⁷ tal with a thickness of 5 μm and a helical pitch of 453.3 nm. It can be seen
¹⁹⁸ from the figure that in the wavelength range from 635 to 725 nm there is a
¹⁹⁹ zone of selective reflection for incident light with right-hand circular polar-
²⁰⁰ ization, while light with left-hand circular polarization does not experience

reflection and passes through the structure unhindered. Thus, a photonic band gap is formed for light with right circular polarization. Conjugation of the defect layer with two cholesterics leads to the appearance in the photonic band gap of a resonance line corresponding to the defect mode (see Figure 1d). The pitch of the cholesteric helix and their thickness were selected in such a way that the wavelength of the resonance line coincided with the absorption wavelength of the thylakoid membrane. As a result, at a wavelength of 680 nm, 11% of the radiation incident on the structure is absorbed in the defective layer. It should be noted that with the same thickness of cholesteric layers the structure is symmetric and the absorptance is the same regardless of whether the radiation falls on the structure through the first cholesteric or through the second. Differences in the absorption spectra of the structure appear when the thicknesses of cholesteric layers are different. To demonstrate this effect, we calculated the reflection, transmission and absorption spectra of the structure for cholesteric thicknesses $L_1 = 2\mu\text{m}$, $L_2 = 3\mu\text{m}$ and $L_1 = 3\mu\text{m}$, $L_2 = 2\mu\text{m}$. The calculation results are shown in figure 2. It can be seen that the absorption coefficient at the resonance wavelength reaches a higher value in the case when light is incident on the structure through a cholesteric of smaller thickness. To determine the structural parameters that provide the greatest absorption at the resonance wavelength, absorption spectra were calculated for different cholesteric thicknesses. The results are shown in Figure 3a. Calculations have shown that the greatest absorption in the defective layer is provided when the thickness of the first cholesteric is equal to 3.2 μm and the thickness of the second cholesteric is greater than 5 μm .

For the proposed structure $\tau_\phi, \tau_{L_1}, \tau_{L_2}$ are defined as:

$$\tau_\phi = \frac{\lambda_f}{4\pi c} \sin^{-2}(\psi/2), \quad (22)$$

$$\tau_{L_1} = \frac{\lambda_f}{4\pi c} \exp\left(\frac{4\pi L_1}{\lambda_f}\right), \quad (23)$$

$$\tau_{L_2} = \frac{\lambda_f}{4\pi c} \exp\left(\frac{4\pi L_2}{\lambda_f}\right), \quad (24)$$

here $\lambda_f = \lambda_0/|n_f|$, $|n_f| = \delta_\varepsilon \sin 2\bar{\chi}$, $\bar{\chi} = (\chi_E + \chi_H)/2$, $\psi = \chi_E - \chi_H$, χ_E and χ_H are the directions of electric and magnetic polarizations.

The relaxation time of the energy into the absorption channel of the defective layer can be determined by comparing the width of the resonance line

231 at non-zero and zero values of the imaginary part of the complex refractive
232 index. The calculation results showed that $1/\tau_{abs} = 0.059$. The dependence
233 of the absorption coefficient of the structure at the resonant wavelength on
234 the thickness of the cholesteric, calculated by the formula (20), is presented
235 in Figure 3b. It should be noted that the results obtained by three different
236 methods have satisfactory agreement.

237 5. Conclusion

238 The results of the calculations show that the transmission of light through
239 a cholesteric liquid crystal does not depend on the direction of propagation.
240 This is due to the Lorentz theorem from 1896, which states that this property
241 should be broken in the absorption spectrum of an asymmetric structure.

242 We calculated the transmission and absorption spectra using three dif-
243 ferent methods: the temporal coupled-mode theory, the anisotropic transfer
244 matrix method, and the Berreman method. Our main findings are:

- 245 • The dependence of the magnitude of resonant absorption of light with
246 right-handed circular polarization in a cholesteric liquid crystal on the
247 position of a defect layer has been demonstrated.
- 248 • Spectra of the highest absorption at the resonant wavelength for various
249 cholesteric thicknesses have been calculated.
- 250 • An increase in absorption, depending on the position of the defect
251 within the cholesteric liquid crystal structure, has been explained using
252 the temporal coupled-mode approach.

253 An advantage of the anisotropic transfer matrix method is that when the
254 matrix is exponentiated to a high degree (for a large number of layers), it
255 reduces to a simple operation of exponentiating the diagonal elements of the
256 matrix. This improves the efficiency of calculating such structures.

257 The work was carried out within the state assignment of the Federal
258 Research Center KSC SB RAS.

259 References

- 260 [1] J. D. Joannopoulos, S. G. Johnson, J. N. Winn, R. D. Meade, Photonic
261 Crystals: Molding the Flow of Light, Second Edition, 2008.

- 262 [2] A. Yariv, P. Yeh, Optical waves in crystals : propagation
263 and control of laser radiation, Wiley-Interscience, 1984. URL:
264 <http://gen.lib.rus.ec/book/index.php?md5=4DD7A9F45FB5883E4BFDB932D3127860>.
- 265 [3] S. I. Azzam, A. V. Kildishev, R.-M. Ma, C.-Z. Ning, R. Oulton,
266 V. M. Shalaev, M. I. Stockman, J.-L. Xu, X. Zhang, Ten years of
267 spasers and plasmonic nanolasers, Light: Science and Applications
268 9 (2020). URL: <http://dx.doi.org/10.1038/s41377-020-0319-7>.
269 doi:10.1038/s41377-020-0319-7.
- 270 [4] J.-C. Huang, Y.-C. Hsiao, Y.-T. Lin, C.-R. Lee, W. Lee, Electrically
271 switchable organo-inorganic hybrid for a white-light laser source, Scientific
272 Reports 6 (2016). URL: <http://dx.doi.org/10.1038/srep28363>.
273 doi:10.1038/srep28363.
- 274 [5] R. Kumari, A. Yadav, B. Lahiri, Photonic crystal all-optical switches,
275 2022. URL: <http://dx.doi.org/10.1002/9781119819264.ch9>.
276 doi:10.1002/9781119819264.ch9.
- 277 [6] T. Li, G. Liu, H. Kong, G. Yang, G. Wei, X. Zhou,
278 Recent advances in photonic crystal-based sensors, Co-
279 ordination Chemistry Reviews 475 (2023) 214909.
280 URL: <http://dx.doi.org/10.1016/j.ccr.2022.214909>.
281 doi:10.1016/j.ccr.2022.214909.
- 282 [7] Y.-C. Hsiao, Hybrid liquid-crystal/photonic-crystal devices: Current
283 research and applications, in: Photonic Crystals - A Glimpse
284 of the Current Research Trends, IntechOpen, 2019, pp. 20130394–
285 20130394. URL: <https://doi.org/10.5772/intechopen.82833>.
286 doi:10.5772/intechopen.82833.
- 287 [8] M. Soljačić, J. D. Joannopoulos, Enhancement of nonlinear effects
288 using photonic crystals, Nature Materials 3 (2004) 211–219. URL:
289 <https://doi.org/10.1038/nmat1097>. doi:10.1038/nmat1097.
- 290 [9] S. G. Moiseev, I. A. Glukhov, Y. S. Dadoenkova, F. F. L.
291 Bentivegna, Polarization-selective defect mode amplification in a
292 photonic crystal with intracavity 2d arrays of metallic nanoparticles,
293 Journal of the Optical Society of America B 36

- 294 (2019) 1645. URL: <https://doi.org/10.1364/josab.36.001645>.
295 doi:10.1364/josab.36.001645.
- 296 [10] S. Y. Vetrov, A. Y. Avdeeva, R. G. Bikbaev, I. Timofeev, Traveling
297 of light through a 1D photonic crystal containing a defect layer with
298 resonant dispersion, Optics and Spectroscopy 113 (2012) 517–521.
299 URL: <http://link.springer.com/10.1134/S0030400X12110070>.
300 doi:10.1134/S0030400X12110070.
- 301 [11] J. P. Vigneron, P. Simonis, Natural photonic crystals,
302 Physica B: Condensed Matter 407 (2012) 4032–4036.
303 URL: <http://dx.doi.org/10.1016/j.physb.2011.12.130>.
304 doi:10.1016/j.physb.2011.12.130.
- 305 [12] R. Vaz, M. F. Frasco, M. G. F. Sales, Photonics in na-
306 ture and bioinspired designs: sustainable approaches for a colour-
307 ful world, Nanoscale Advances 2 (2020) 5106–5129. URL:
308 <http://dx.doi.org/10.1039/DONA00445F>. doi:10.1039/d0na00445f.
- 309 [13] G. I. Waterhouse, M. R. Waterland, Opal and inverse opal pho-
310 tonic crystals: Fabrication and characterization, Polyhedron 26 (2007)
311 356–368. URL: <http://dx.doi.org/10.1016/j.poly.2006.06.024>.
312 doi:10.1016/j.poly.2006.06.024.
- 313 [14] V. Zaytsev, T. I. Ermakov, F. S. Fedorov, N. Balabin, P. O.
314 Kapralov, J. V. Bondareva, D. O. Ignatyeva, B. N. Khlebtsov, S. S.
315 Kosolobov, V. I. Belotelov, A. G. Nasibulin, D. A. Gorin, De-
316 sign of an artificial opal/photonic crystal interface for alcohol in-
317 toxication assessment: Capillary condensation in pores and photonic
318 materials work together, Analytical Chemistry 94 (2022) 12305–
319 12313. URL: <http://dx.doi.org/10.1021/acs.analchem.2c00573>.
320 doi:10.1021/acs.analchem.2c00573.
- 321 [15] F. Fathi, H. Monirinasab, F. Ranjbari, K. Nejati-Koshki, Inverse opal
322 photonic crystals: Recent advances in fabrication methods and biological
323 applications, Journal of Drug Delivery Science and Technology 72 (2022)
324 103377. URL: <http://dx.doi.org/10.1016/j.jddst.2022.103377>.
325 doi:10.1016/j.jddst.2022.103377.

- 326 [16] R. C. McPhedran, N. A. Nicorovici, D. R. McKenzie, L. C. Bot-
327 ten, A. R. Parker, G. W. Rouse, The sea mouse and the pho-
328 tonic crystal, *Australian Journal of Chemistry* 54 (2001) 241. URL:
329 <http://dx.doi.org/10.1071/CH01054>. doi:10.1071/ch01054.
- 330 [17] L. Biro, K. Kertesz, Z. Vertes, G. Mark, Z. Balint, V. Lousse, J.-P.
331 Vigneron, Living photonic crystals: Butterfly scales – nanostructure
332 and optical properties, *Materials Science and Engineering: C* 27 (2007)
333 941–946. URL: <http://dx.doi.org/10.1016/j.msec.2006.09.043>.
334 doi:10.1016/j.msec.2006.09.043.
- 335 [18] C. P. Barrera-Patino, J. D. Vollet-Filho, R. G. Teixeira-Rosa, H. P.
336 Quiroz, A. Dussan, N. M. Inada, V. S. Bagnato, R. R. Rey-
337 Gonzalez, Photonic effects in natural nanostructures on mor-
338 pho cypris and greta oto butterfly wings, *Scientific Reports*
339 10 (2020). URL: <http://dx.doi.org/10.1038/s41598-020-62770-w>.
340 doi:10.1038/s41598-020-62770-w.
- 341 [19] S. Vignolini, E. Moyroud, B. J. Glover, U. Steiner, Analysing photonic
342 structures in plants, *Journal of The Royal Society Interface* 10 (2013)
343 20130394. URL: <http://dx.doi.org/10.1098/rsif.2013.0394>.
344 doi:10.1098/rsif.2013.0394.
- 345 [20] M. Jacobs, M. Lopez-Garcia, O.-P. Phrathep, T. Lawson, R. Oulton,
346 H. M. Whitney, Photonic multilayer structure of begonia chloro-
347 plasts enhances photosynthetic efficiency, *Nature plants* 2 (2016) 16162.
348 doi:10.1038/nplants.2016.162.
- 349 [21] P. S. Pankin, A. V. Shabanov, D. N. Maksimov, S. V. Nabol,
350 D. S. Buzin, A. I. Krasnov, G. A. Romanenko, V. S. Sutormin,
351 V. A. Gunyakov, F. V. Zelenov, A. N. Masyugin, V. P. Vyatkin,
352 I. V. Nemtsev, M. N. Volochaev, S. Y. Vetrov, I. V. Timofeev,
353 Asymmetric resonant light absorption in a chloroplast microstructure,
354 *Journal of the Optical Society of America B* 40 (2022) 87. URL:
355 <https://doi.org/10.1364/josab.477110>. doi:10.1364/josab.477110.
- 356 [22] M. A. Castillo, W. P. Wardley, M. Lopez-Garcia, Light-dependent mor-
357 phological changes can tune light absorption in iridescent plant chloro-
358 plasts: A numerical study using biologically realistic data, *ACS Photonics* 8 (2021) 1058–1068. doi:10.1021/acsphtronics.0c01600.
359

- 360 [23] Melentiev, Pavel N., Afanasiev, Anton E., Kalmykov,
361 Alexey S., Balykin, Victor I., Light transmission asym-
362 metry and optical diode*, Eur. Phys. J. D 71 (2017)
363 152. URL: <https://doi.org/10.1140/epjd/e2017-70803-9>.
364 doi:10.1140/epjd/e2017-70803-9.
- 365 [24] D. Jalas, A. Petrov, M. Eich, W. Freude, S. Fan, Z. Yu,
366 R. Baets, M. Popovic, A. Melloni, J. D. Joannopoulos, M. Van-
367 wolleghem, C. R. Doerr, H. Renner, What is – and what
368 is not – an optical isolator, Nature Photonics 7 (2013)
369 579–582. URL: <https://doi.org/10.1038/nphoton.2013.185>.
370 doi:10.1038/nphoton.2013.185.
- 371 [25] V. A. Belyakov, A. S. Sonin, Optika kholestericheskikh zhidkikh
372 kristallov [Optics of choltsteric liquid crystals], Moscow: Nauka Publ.,
373 1982.
- 374 [26] V. A. Belyakov, Diffraction Optics of Complex-Structured Periodic Me-
375 dia: Localized Optical Modes of Spiral Media, Springer International
376 Publishing, M, 2019.
- 377 [27] D. V. Shmeliova, V. A. Belyakov, Director distribution in
378 Grandjean-Cano wedge and restoration of surface anchoring
379 potential, Mol. Cryst. Liq. Cryst. 646 (2017) 160–167.
380 URL: <http://dx.doi.org/10.1080/15421406.2017.1287399>.
381 doi:10.1080/15421406.2017.1287399.
- 382 [28] M. V. Gorkunov, A. R. Geivandov, A. V. Mamonova, I. V.
383 Simdyankin, I. V. Kasyanova, A. A. Ezhov, V. V. Artemov,
384 Non-Mechanical Multiplexed Beam-Steering Elements Based
385 on Double-Sided Liquid Crystal Metasurfaces, Photonics 9
386 (2022) 986. URL: <https://www.mdpi.com/2304-6732/9/12/986>.
387 doi:10.3390/photonics9120986.
- 388 [29] A. Alodjants, A. Y. Leksin, A. Prokhorov, S. Arakelian,
389 Quantum Limit for Observation of Self-switching Effect of
390 Light in Nonlinear Spatially Inhomogeneous Optical Sys-
391 tem, Mol. Cryst. Liq. Cryst. 375 (2002) 185–194. URL:
392 <http://www.informaworld.com/openurl?genre=article&doi=10.1080/713738331&magic=doi:10.1080/713738331>.

- 394 [30] P. V. Dolganov, Luminescence spectra of a cholesteric
395 photonic crystal, JETP Lett. 105 (2017) 657–660. URL:
396 <http://link.springer.com/10.1134/S002136401710006X>.
397 doi:10.1134/S002136401710006X.
- 398 [31] N. Masters, M. Lopez Garcia, R. Oulton, H. Whitney, Characterization
399 of chloroplast iridescence in selaginella erythropus, Journal of the Royal
400 Society Interface 15 (2018). doi:10.1098/rsif.2018.0559.
- 401 [32] A. Capretti, A. Ringsmuth, J. van Velzen, A. Rosnik, R. Croce,
402 T. Gregorkiewicz, Nanophotonics of higher-plant photosynthetic
403 membranes, Light: Science and Applicationsh 5 (2019) 1–13.
404 doi:<https://doi.org/10.1038/s41377-018-0116-8>.
- 405 [33] P. A. Yeh, Electromagnetic propagation in birefringent layered me-
406 dia, Journal of the Optical Society of America 69 (1979) 742–756.
407 URL: <https://api.semanticscholar.org/CorpusID:122299703>.
408 doi:10.1364/JOSA.69.000742.
- 409 [34] M. A. Korshunov, A. V. Shabanov, E. R. Bukhanov, V. F. Sha-
410 banov, The theory of liquid crystals, Doklady Physics 63 (2018) 1–4.
411 doi:10.1134/S1028335818010068.
- 412 [35] C. W. Oseen, The theory of liquid crystals, Trans. Faraday Soc. 29
413 (1933) 883–899. doi:10.1039/TF9332900883.
- 414 [36] D. Fedchenko, N. Tarkhanov, A class of toeplitz operators in sev-
415 eral variables, Advances in Applied Clifford Algebras 25 (2015) 811.
416 doi:10.1103/PhysRevE.76.031701.
- 417 [37] A. Gevorgyan, A. Kocharian, G. Vardanyan, Accumulation
418 and transmission of the light energy in nonreciprocal multi-
419 layer systems, Optics Communications 259 (2006) 455–464. URL:
420 <https://www.sciencedirect.com/science/article/pii/S003040180500965X>.
421 doi:<https://doi.org/10.1016/j.optcom.2005.09.025>.
- 422 [38] A. H. Gevorgyan, M. Z. Harutyunyan, Chiral photonic crystals
423 with an anisotropic defect layer, Phys. Rev. E 76 (2007) 031701.
424 doi:10.1103/PhysRevE.76.031701.

- 425 [39] A. Gevorgyan, Chiral photonic crystals with an anisotropic defect layer:
426 Oblique incidence, Optics Communications 281 (2008) 5097–5103. URL:
427 <https://www.sciencedirect.com/science/article/pii/S0030401808006718>.
428 doi:<https://doi.org/10.1016/j.optcom.2008.07.024>.
- 429 [40] D. W. Berreman, Optics in stratified and anisotropic media: 4x4-
430 matrix formulation, Journal of the Optical Society of America
431 62 (1972) 502. URL: <https://doi.org/10.1364/josa.62.000502>.
432 doi:10.1364/josa.62.000502.
- 433 [41] H. A. Haus, Waves and Fields in Optoelectronics, Prentice Hall, 1983.
434 URL: <http://www.tandfonline.com/doi/abs/10.1080/716099690>.